

Discrete Element Method simulations of the saturation of aeolian sand transport

Thomas Pähtz,^{1,2} Amir Omeradžić,³ Marcus V. Carneiro,³ Nuno A. M. Araújo,^{4,5} and Hans J. Herrmann^{3,6}

The saturation length of aeolian sand transport (L_s), characterizing the distance needed by wind-blown sand to adapt to changes in the wind shear, is essential for accurate modeling of the morphodynamics of Earth's sandy landscapes and for explaining the formation and shape of sand dunes. In the last decade, it has become a widely-accepted hypothesis that L_s is proportional to the characteristic distance needed by transported particles to reach the wind speed (the “drag length”). Here we challenge this hypothesis. From extensive numerical Discrete Element Method simulations, we find that, for medium and strong winds, $L_s \propto V_s^2/g$, where V_s is the saturated value of the average speed of sand particles traveling above the surface and g the gravitational constant. We show that this proportionality is consistent with a recent analytical model, in which the drag length is just one of four similarly important length scales relevant for sand transport saturation.

1. Introduction

Aeolian transport of sand occurs when a sufficiently strong wind blows over a sand bed [Bagnold, 1941; Shao, 2008; Durán et al., 2011; Kok et al., 2012]. The two dominant transport modes are saltation, referring to particles hopping along the sand surface in characteristic trajectories [Bagnold, 1941], and creep, referring to particles rolling and sliding along the sand surface [Bagnold, 1937]. Wind-blown, initially flat sand beds may evolve into bedforms, such as ripples and dunes, due to different kinds of instabilities [Claudin and Andreotti, 2006; Andreotti et al., 2010; Fourrière et al., 2010; Parteli et al., 2011; Charru et al., 2013; Durán et al., 2014a].

For instance, dunes are thought to form due to an aerodynamic instability, namely a slight phase difference between topography and wind shear maxima on a periodically perturbed sand bed [Jackson and Hunt, 1975; Hunt et al., 1988;

Kroy et al., 2002a, b]. If this phase difference is larger than the phase difference between sand transport and wind shear maxima, which is characterized by the saturation length (L_s) [Sauermann et al., 2001; Parteli and Herrmann, 2007a; Andreotti et al., 2010; Pähtz et al., 2013, 2014], the perturbations grow. This is one of the reasons why L_s plays an important role in aeolian dune formation. Indeed, L_s controls the length of the smallest (“elementary”) dunes evolving from a flat sand bed and the minimal size of crescent-shaped barchans [Parteli et al., 2007; Claudin and Andreotti, 2006; Fourrière et al., 2010]. In contrast, the steady state dune dimensions are controlled by the aerodynamic roughness (z_o^*) [Pelletier, 2009]. L_s is also a key parameter in morphodynamic models of Earth's sandy landscapes, such as aeolian dune models [Kroy et al., 2002a, b; Schwämmle and Herrmann, 2003; Parteli and Herrmann, 2007b; Narteau et al., 2009; Parteli et al., 2009, 2014].

It has been a challenging task to predict L_s as a function of wind and particle parameters, such as the wind shear velocity (u_*), the mean particle diameter (d), the particle (ρ_p) and fluid density (ρ_f), and the kinematic air viscosity (ν). In fact, the main difficulty has been to understand which of the involved relaxation mechanism is the slowest and thus the most important one. Sauermann et al. [2001] derived an expression for L_s based on the assumption that L_s corresponds to the length needed to eject particles from the sand bed. Based on measurements of the size of both subaqueous and aeolian barchan dunes, Hersen et al. [2002] proposed that L_s is proportional to the drag length ($L_d = (\rho_p/\rho_f)d$), which characterizes the distance transported particles need to reach the flow speed. Estimations of the wavelength of elementary dunes by Claudin and Andreotti [2006] and measurements by Andreotti et al. [2010] later supported this proposition. Indeed, these measurements confirmed that L_s is approximately proportional to d and essentially independent of u_* , as predicted by $L_s \propto L_d$. However, there is considerable room for alternative interpretations of these measurements. The analytical model for the saturation length of both subaqueous and aeolian particle transport recently proposed by Pähtz et al. [2013, 2014] is also consistent with these measurements (without fitting), even though the model predicts that L_s varies with u_* . In this model, the four potentially most important relaxation mechanisms are all accounted for (ejection of bed particles and particle deceleration in particle-bed collisions, fluid drag acceleration of particles, relaxation of the fluid speed), and it turns out that neglecting any of them entirely changes the model predictions [Pähtz et al., 2014]. This shows that the identity of the most important relaxation mechanisms remains an open problem.

Here we use Discrete Element Method (DEM) simulations for the particle phase to investigate aeolian sand transport saturation. This modeling technique considers interparticle interactions above and also with the sand bed and is thus more realistic than older modeling techniques [e.g., Almeida et al., 2007, 2008; Kok and Renno, 2009], which usually consider the sand bed as a flat, rough wall. However, it is also

¹Institute of Physical Oceanography, Ocean College, Zhejiang University, 310058 Hangzhou, China

²State Key Laboratory of Satellite Ocean Environment Dynamics, The Second Institute of Oceanography, 310012 Hangzhou, China

³Institut für Baustoffe, ETH Zürich, 8093 Zurich, Switzerland

⁴Departamento de Física, Faculdade de Ciências, Universidade de Lisboa, P-1749-016 Lisboa, Portugal

⁵Centro de Física Teórica e Computacional, Universidade de Lisboa, Avenida Professor Gama Pinto 2, P-1649-003 Lisboa, Portugal

⁶Departamento de Física, Universidade Federal do Ceará, 60451-970 Fortaleza, Ceará, Brazil

computationally more costly, which is the main reason why this technique had not been used for modeling particle-laden flows until a few years ago [Carneiro et al., 2011; Durán et al., 2012; Carneiro et al., 2013; Durán et al., 2014b, a; Schmeckle, 2014; Pähitz et al., 2015]. From our simulations, we find that the total mass of particles transported above the sand bed (M) relaxes significantly slower towards its saturated value (M_s) than the average particle velocity above the sand bed ($V = Q/M$, where Q is the sand transport rate above the sand bed) towards its saturated value (V_s), indicating that the drag length is not the dominant saturation length scale. Moreover, we find that $L_s \propto V_s^2/g$, where g is the gravitational constant, when $u_* > 4u_t$, where u_t is the dynamic threshold of sand transport (i.e., the extrapolated value of u_* at which the saturated sand transport rate (Q_s) vanishes). This finding is consistent with the analytical model by Pähitz et al. [2013, 2014], supporting the hypothesis that the aforementioned four potentially most important relaxation mechanisms are all similarly relevant.

This paper is organized as follows. First, we present the modeling technique we used to simulate aeolian particle transport in Section 2. Afterwards we show our numerical results in Section 3, which are then discussed and compared with the analytical model for the saturation length recently proposed by Pähitz et al. [2013, 2014] in Section 4. Finally, we draw conclusions in Section 5.

2. Modeling technique

In this section, we briefly describe the three-dimensional numerical model which we used to model sand transport. A more detailed description can be found in Carneiro et al. [2013], particularly its supplementary material.

For the computation of the mean horizontal wind velocity (u), the model uses the mixing-length approximation of the Reynolds-averaged Navier-Stokes equations (neglecting viscous wind shear), where the mixing length is given by $\kappa(z-h)$ with $\kappa = 0.4$ being the von Karmán constant and $z-h$ characterizing the vertical distance from the top of the sand bed ($z=h$). This reads [Carneiro et al., 2013]

$$\frac{du}{dz} = \frac{u_*}{\kappa(z-h)} \sqrt{1 - \frac{1}{\rho_f u_*^2} \int_z^\infty f dz}. \quad (1)$$

The term containing f , the horizontal drag force per unit volume applied by the wind on the particles (the drag law by Cheng [1997] is used), takes into account that the wind speed is reduced due to continuous transfer of momentum from wind to particles. The integration of Eq. (1) starts at height $z = h + z_o$, where $z_o = d/30$ is the aerodynamic roughness of the sand bed as it would be in the absence of sand transport, corresponding to aerodynamically rough flow [Bagnold, 1941]. However, during sand transport, the reduced wind speed at the top of the saltation layer corresponds to an increased roughness value (z_o^*).

It is important to note that Eq. (1) is applied to calculate the wind velocity profile at every time step because we assume that the flow adapts to local drag decelerations of the wind speed within the integration time ($\Delta t = 0.005$ s). This standard assumption led to several previous numerical results in agreement with experiments [Carneiro et al., 2011; Durán et al., 2012; Carneiro et al., 2013; Durán et al., 2014b; Pähitz et al., 2015]. Nevertheless, we argue why it is reasonable to make such assumption in the following.

There are actually two time scales involved. First, the time needed to transmit the drag force between fluid and particles. As the drag force is transmitted via collisions between air molecules (which are extremely small) and the

sand grains, this time scale is much smaller than the integration time. The second time scale is related to the propagation of this perturbation to the entire system. As perturbations of a fluid typically travel at the speed of sound (in air, $c \approx 340$ m/s) and the maximum distance they need to travel to reach all relevant locations of the simulated saltation layer is of the order of $100d = 0.02$ m (the height of the saltation layer), the maximal time needed for this perturbation to influence all relevant locations of the simulated saltation layer is around 0.0006 s, which is around a factor 10 smaller than Δt and around a factor 10^3 smaller than the saturation time. Even if the necessary time for the flow to accommodate to a perturbation is larger than the necessary time a perturbation needs to travel to reach all relevant locations, it is hard to imagine that this time comes any close to the saturation time. Moreover, since particle and flow velocity are of the same order of magnitude, also the length needed for the flow to adapt to the perturbation should be much smaller than the saturation length.

Trajectories and velocities of particles are obtained from solving Newton's equations of motion through the velocity-Störmer-Verlet scheme [Griebel et al., 2007], considering gravity and wind drag as the external forces acting on the particles. Interparticle contacts are modeled through a dissipative spring dashpot potential (coefficient of restitution, $e = 0.65$), while frictional contacts are neglected (no particle rotation). The system dimensions are length \times height \times width = $50d \times 400d \times 7.5d$, and 1410 particles with normally distributed diameters ($d_p = (1 \pm 0.1)d$) are simulated. Most of these particles constitute a bed of around twelve particle layers. This is sufficiently thick to suppress the reflection of shock waves from the dissipative ($e = 0.5$) bottom wall [Rioual et al., 2000, 2003]. The simulation top is open and the side boundaries periodic. In fact, particles never reach the top of the system.

3. Results

Using the model described in Section 2, we carried out simulations for typical sand transport conditions on Earth

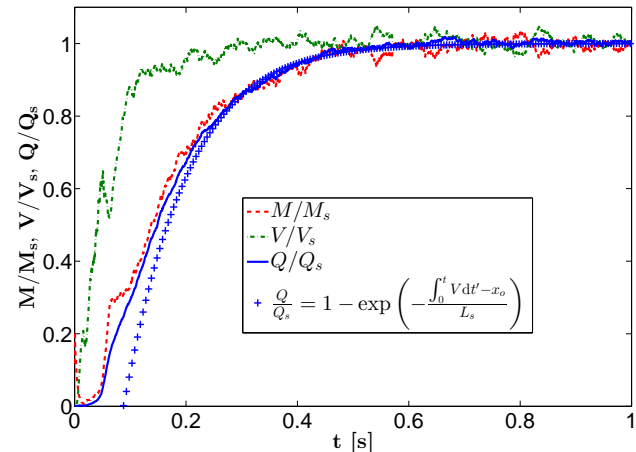


Figure 1. Time evolution of M/M_s (red, dashed line), V/V_s (green, dash-dotted line), and Q/Q_s (blue, solid line) obtained from simulations of typical sand transport conditions on Earth ($g = 9.81$ m/s², $d = 200$ μ m, $\rho_p = 2650$ kg/m³, $\rho_f = 1.174$ kg/m³, $\nu = 1.59 \times 10^{-5}$ m²/s) with $u_* = 1.2$ m/s. The blue crosses correspond to the best fit of Eq. (5) to the data [Q/Q_s](t) near saturation ($|1 - Q/Q_s| < 0.2$). The analogous plots for different values of u_* look similar.

($g = 9.81 \text{ m/s}^2$, $d = 200 \text{ }\mu\text{m}$, $\rho_p = 2650 \text{ kg/m}^3$, $\rho_f = 1.174 \text{ kg/m}^3$, $\nu = 1.59 \times 10^{-5} \text{ m}^2/\text{s}$). For these conditions, we varied u_* between two and nearly ten times the threshold shear velocity ($u_t = 0.195 \text{ m/s}$). For each u_* , 15 runs were performed, starting from different initial condition. Indeed, while the sand bed in all samples was exactly the same at the start of each simulation ($t = 0$), ten particles with velocity $v_x = v_z = 1 \text{ m/s}$ were randomly placed sufficiently high above the surface ($z > h + 20d$). Each of these samples evolved in time towards the saturated state. The supplementary online material contains a movie showing the time evolution of a given sample ($u_* = 0.8 \text{ m/s}$) between $t = 0$ and $t = 0.35 \text{ s}$.

From averaging the particle locations and velocities over the 15 samples corresponding to each u_* and further over the horizontal (x) and lateral (y) direction, we obtain the vertical profiles of the local mass density (ρ) and the mass-weighted average particle velocity $\langle \mathbf{v} \rangle$ the particle velocity at each time. The time evolution of $M = \int_h^\infty \rho dz$ (red, dashed line), $Q = \int_h^\infty \rho \langle v_x \rangle dz$ (blue, solid line), and $V = Q/M$ (green, dash-dotted line) further obtained from these profiles relative to their saturated values is plotted in Fig. 1 for $u_* = 1.2 \text{ m/s}$ (for different u_* , it looks similar). It can be seen that the time transient behavior of Q is similar to that determined in older studies [Spies *et al.*, 2000; Ma and Zheng, 2011]. Furthermore, one immediately recognizes that M relaxes significantly slower towards M_s than V towards V_s (this is also true for our simulations with other values of u_*). This means that our simulations do not confirm the hypothesis that drag is the dominant mechanism controlling sand transport saturation, which would instead require that M always relaxes much faster towards M_s than V towards V_s [Pächtz *et al.*, 2014]. Moreover, this observation can be used to extract the saturation length (L_s) from the time evolution of Q , as we explain in the following.

Mathematically, L_s has its origin in the mass conservation equation, which in its local form reads

$$\frac{\partial \rho}{\partial t} + \frac{\partial \rho \langle v_x \rangle}{\partial x} + \frac{\partial \rho \langle v_y \rangle}{\partial y} + \frac{\partial \rho \langle v_z \rangle}{\partial z} = 0. \quad (2)$$

Indeed, L_s is typically defined through a first-order Taylor expansion of the rate of relaxation ($\Gamma(Q)$) of Q around Q_s [Andreotti *et al.*, 2010; Pähtz *et al.*, 2013, 2014],

$$\frac{dQ}{dx} = \Gamma(Q) \simeq \frac{Q_s - Q}{L_s}, \quad (3)$$

which, using $\Gamma = [\rho \langle v_z \rangle](h)$, is the height integration ($\int_h^\infty \cdot dz$) of Eq. (2) for steady and laterally homogeneous conditions ($\partial/\partial t = \partial/\partial y = 0$). Since $\Gamma(Q_s) = 0$, L_s corresponds to the negative inverse Taylor coefficient ($-\Gamma'(Q_s)$). By definition Eq. (3), describing the spatial relaxation of Q towards Q_s , is only applicable near saturation ($|1 - Q/Q_s| \ll 1$).

Since our simulations correspond to spatially and laterally homogeneous conditions ($\partial/\partial x = \partial/\partial y = 0$), height integration of Eq. (2) yields

$$\frac{dQ}{V dt} \simeq \frac{dM}{dt} = \Gamma(Q) \simeq \frac{Q_s - Q}{L_s}, \quad (4)$$

where the approximation on the left hand side uses that M relaxes significantly slower towards M_s than V towards V_s . From comparison between Eqs. (3) and (4), it is apparent that the saturation in t in our simulations is equivalent to a saturation in x if $x = \int_0^t V dt'$ (i.e., $d/dx = V/dt$) is used to relate them. In fact, fitting (nonlinear least squares method) Q_s , x_o , and L_s to best agreement with the analytic

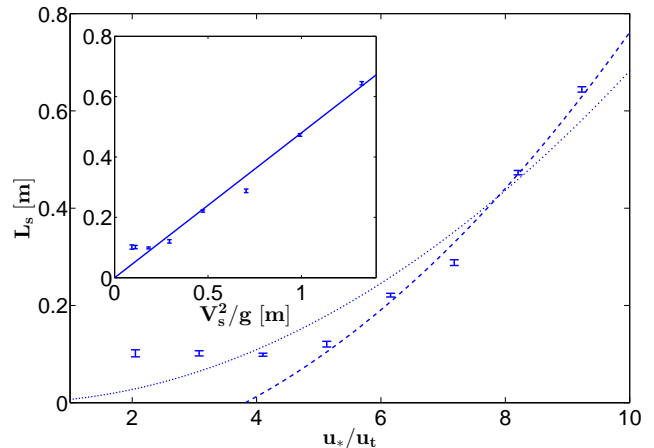


Figure 2. The saturation length (L_s) as a function of u_*/u_t (symbols) obtained from simulations of typical sand transport conditions on Earth ($g = 9.81 \text{ m/s}^2$, $d = 200 \text{ }\mu\text{m}$, $\rho_p = 2650 \text{ kg/m}^3$, $\rho_f = 1.174 \text{ kg/m}^3$, $\nu = 1.59 \times 10^{-5} \text{ m}^2/\text{s}$), whereby the dashed line corresponds to $L_s = 2.30 u_*^2/g - 0.13 \text{ m}$ and the dotted line to $L_s = 1.76 u_*^2/g$. The inset shows L_s as a function of V_s^2/g for the same conditions, whereby the solid line corresponds to $L_s = 0.48 V_s^2/g$. The error bars correspond to the 95%-confidence intervals obtained from the best fits to Eq. (5).

solution

$$\frac{Q}{Q_s} = 1 - \exp\left(-\frac{\int_0^t V dt' - x_o}{L_s}\right) \quad (5)$$

of Eq. (4) (since Q_s does not depend on t for constant wind shear) allows us to determine L_s from our simulations (see blue crosses in Fig. 1).

Fig. 2 shows L_s as a function of u_*/u_t obtained from our simulations, whereby the error bars correspond to the 95%-confidence intervals obtained from the best fits to Eq. (5). It can be seen that L_s remains nearly constant between $2u_t$ and $4u_t$, qualitatively consistent with measurements [Andreotti *et al.*, 2010]. However, L_s increases with u_* when $u_* > 4u_t$. This increase within the error bars follows the scaling relation

$$L_s = \alpha V_s^2/g, \quad (6)$$

as shown in the inset of Fig. 2, where $\alpha = 0.48$. Interestingly, while the scaling $L_s \propto V_s^2/g$ describes the data with $u_* > 4u_t$ very well, the scaling $L_s \propto u_*^2/g$ does not (see the dotted line in Fig. 2, corresponding to the best fit of $L_s \propto u_*^2/g$ to data with $u_*/u_t > 4$), indicating that V_s and not u_* is the relevant parameter controlling L_s . Only when one allows a small offset, a good fit can be obtained. This is shown by the dashed line in Fig. 2, which corresponds to $L_s + L_{so} \propto u_*^2/g$, where the offset ($L_{so} = 0.13 \text{ m}$) is expected to have a complex dependency on particle and wind parameters (except u_*).

4. Discussion

In this section, we first briefly describe the analytical model for the saturation length proposed by Pähtz *et al.* [2013, 2014] in Section 4.1. We then compare the model

predictions with our numerical results shown in Fig. 2 and with the scaling in Eq. (6).

4.1. Analytical model by Pächtz et al. [2013, 2014]

The analytical model for the saturation length by Pächtz et al. [2013, 2014] takes into account that M and V relax towards M_s and V_s , respectively, due to different relaxation mechanisms. Changes in M are controlled by the ejection of bed particles in particle-bed collisions [Kok et al., 2012], while changes in V are driven by the acceleration of transported particles due to fluid drag and their deceleration in particle-bed collisions. On the one hand, the changes of V were explicitly modeled within the momentum balance: the fluid drag acceleration through the fluid drag law by Julien [1995] for natural sand and the deceleration in particle-bed collisions by means of a Coulomb friction law, assuming a proportionality between average horizontal and vertical forces acting on transported particles. This assumption is well established in the literature as it leads to the experimentally [Creysseles et al., 2009] and numerically [Kok and Renno, 2009; Pächtz et al., 2012] confirmed relation

$$M_s = \frac{\rho_f}{\mu g} (u_*^2 - u_t^2), \quad (7)$$

where $\mu \approx 1$ (from experimental data [Creysseles et al., 2009; Pächtz et al., 2012]) is the associated Coulomb friction coefficient. On the other hand, changes in M were not explicitly modeled, but implicitly accounted for in the parameter

$$c_M = \frac{V_s}{M_s} \frac{dM}{dV}(V_s), \quad (8)$$

which describes the relative change of M with V near the saturated regime [Pächtz et al., 2014]. Moreover, taking into account that not only M and V , but also the average wind speed (U) relaxes towards its saturated value, led to the introduction of another parameter c_U , describing the relative change of U with the bed fluid shear velocity (i.e., the value of the fluid shear velocity at the bed, which is smaller than u_* due to momentum transfer from fluid to particles). The parameters c_M and c_U were by far the most uncertain model parameters as they were the only ones not determined by measurements, but instead by theoretical arguments (which led to $c_M \approx c_U \approx 1$ for aeolian sand transport) [Pächtz et al., 2013, 2014]. However, in the limit of large fluid shear velocities ($u_*/u_t \gg 1$), the model becomes independent of c_U . Indeed, in this limit, the final model equation for L_s reads [Pächtz et al., 2014],

$$L_s = \frac{(2 + c_M)c_v}{c_M\mu} \frac{V_s^2}{g}, \quad (9)$$

where $c_v \approx 1.3$ (from experimental data [Rasmussen and Sørensen, 2008; Creysseles et al., 2009; Pächtz et al., 2013, 2014]) is the saturated value of $\int_h^\infty \rho \langle v_x^2 \rangle dz / (MV^2)$.

4.2. Comparison between analytical and numerical model predictions

It can be seen that Eq. (2) predicts $L_s \propto V_s^2/g$, which resembles the scaling in Eq. (6) obtained from our simulations. Since both equations are only valid for sufficiently large values u_*/u_t , this resemblance supports the analysis by Pächtz et al. [2013, 2014]. In this analysis, the four potentially most important relaxation mechanisms are all accounted for (ejection of bed particles and particle deceleration in particle-bed collisions, fluid drag acceleration of particles, relaxation of

the fluid speed), as described in Section 4.1. Since neglecting any of them entirely changes the model predictions [Pächtz et al., 2014], the resemblance between the analytical and numerical model predictions suggests that these four relaxation mechanisms are all similarly relevant. This is just another indication that L_d is *not* the dominant length scale controlling sand transport saturation.

However, one must also note that there are differences between these models. First, the qualitative model predictions for small u_*/u_t slightly differ from each other. While the numerical model predicts that L_s remains nearly constant between $2u_t$ and $4u_t$, the analytical model predicts a slight increase with u_* [Pächtz et al., 2013, 2014]. This might be a result of the aforementioned uncertainty of the parameter c_U . Second, while the analytical model predictions are consistent with the measurements by Andreotti et al. [2010], the numerical model predictions shown in Fig. 2 are not. This can be entirely linked to differences in the model parameters μ and c_M , as we explain in the following. First, from fitting Eq. (7) to our numerical data (it fits very well, not shown), we obtain $\mu \approx 2$, in contrast to $\mu \approx 1$, which Pächtz et al. [2013, 2014] obtained from experimental data. Second, since M relaxes much slower towards M_s than V towards V_s in the simulations (see Fig. 1), c_M becomes very large, while $c_M \approx 1$ was estimated by Pächtz et al. [2013, 2014] from theoretical arguments. In fact, using $\mu \approx 2$ and $c_M \rightarrow \infty$ in Eq. (2) yields the prefactor $(2 + c_M)c_v / (c_M\mu) \rightarrow \approx 0.65$ close to the prefactor $\alpha = 0.48$ in Eq. (6). This means the numerical model and the analytical model seem quantitatively consistent with each other since the differences in the parameters μ and c_M are likely the results of simplifications in the numerical model. For instance, the difference in the value of μ between simulations and measurements can be linked to the interparticle contact model, which is known to have considerable influence on the frictional behavior of solids [Campbell, 2006]. Indeed, the model neglects particle rotation and uses rather soft particles (stiffness $k = 1\text{kg/s}^2$), which allows particle overlaps of about 20%, while in reality the stiffness is several orders of magnitude larger. Also, the coefficient of restitution used in our simulations ($e = 0.65$) might have been too small. Comparable studies usually use larger values [e.g., Durán et al., 2012, $e = 0.9$] and obtain a Coulomb friction coefficients near unity.

5. Conclusion

We simulated aeolian sand transport using DEM simulations. From these simulations, we obtained the saturation curves in Fig. 1 of the total mass of particles transported above the sand bed (M), their average velocity (V), and the associated sand flux ($Q = MV$). These numerical data indicate that M saturates much slower than V , challenging the widely-accepted hypothesis that the drag length ($L_d = (\rho_p/\rho_f)d$) is the dominant length scale controlling aeolian sand transport saturation, which would require the opposite, namely that M saturates much faster than V . Since L_d does not change with u_* , the same hypothesis is further challenged by the numerical data in Fig. 2 showing that the saturation length (L_s) significantly increases with the wind shear velocity (u_*) for medium and strong winds ($u_* > 4u_t$). Moreover, this increase follows the scaling relation $L_s \propto V_s^2/g$ (see inset of Fig. 2), qualitatively consistent with the limit $u_*/u_t \gg 1$ of the recently proposed analytical model by Pächtz et al. [2013, 2014]. In Section 4, we showed that this analytical model also predicts the proportionality factor in $L_s \propto V_s^2/g$ to be about 0.65, which is close to the numerically obtained value $\alpha = 0.48$. This adds another piece of doubt on a dominating role of L_d because the model accounts for the four potentially most important relaxation

mechanisms (ejection of bed particles and particle deceleration in particle-bed collisions, fluid drag acceleration of particles, relaxation of the fluid speed), and neglecting any of them entirely changes the model predictions [Pächtz et al., 2014].

The scaling relation $L_s \propto V_s^2/g$, found for medium and strong winds, might itself become an important step towards modeling of dune and dune field evolutions in sand storms. For this purpose, one would need a model predicting V_s . In fact, there are a considerable number of analytical models predicting V_s as function of u_* [e.g., Bagnold, 1941; Kawamura, 1951; Owen, 1964; Bagnold, 1973; Kind, 1976; Lettau and Lettau, 1978; Ungar and Haff, 1987; Sørensen, 1991, 2003; Durán et al., 2011; Pähtz et al., 2012; Lämmel et al., 2012], some of them might be applicable to sand storm conditions.

Finally, it is worth to note that aeolian dunes are often superimposed by ripples. Compared to the flat sand bed condition present in our simulation, the presence of such ripples leads to a strong increase of the aerodynamic roughness (z_o^*), which corresponds to a smaller wind and thus saturated particle velocity (V_s) in the saltation layer. The relation $L_s \propto V_s^2/g$, found for medium and strong winds, would thus imply that the formation of superimposed ripples on the surface of aeolian dunes is associated with a simultaneous decrease of L_s .

Acknowledgments. The data displayed in Figs. 1 and 2 are available from the authors. This work was partially supported by the National Natural Science Foundation of China (Grant No. 41350110226), the Brazilian Council for Scientific and Technological Development CNPq, ETH (Grant No. ETH-10 09-2), the European Research Council (Grant No. FP7-319968), and the Portuguese Foundation for Science and Technology (FCT) under Contracts nos. EXCL/FIS-NAN/0083/2012, PEst-OE/FIS/UI0618/2014, and IF/00255/2013.

References

- Almeida, M. P., J. S. Andrade, and H. J. Herrmann (2007), Aeolian transport of sand, *The European Physical Journal E*, *22*, 195–200.
- Almeida, M. P., E. J. R. Parteli, J. S. Andrade, and H. J. Herrmann (2008), Giant saltation on mars, *Proceedings of the National Academy of Science*, *105*(17), 6222–6226, doi:10.1073/pnas.0800202105.
- Andreotti, B., P. Claudin, and O. Pouliquen (2010), Measurements of the aeolian sand transport saturation length, *Geomorphology*, *123*, 343–348.
- Bagnold, R. A. (1937), The transport of sand by wind, *The Geographical Journal*, *89*(5), 409–438, doi:10.2307/1786411.
- Bagnold, R. A. (1941), *The physics of blown sand and desert dunes*, Methuen, New York.
- Bagnold, R. A. (1973), The nature of saltation and “bed-load” transport in water, *Proceedings of the Royal Society London Series A*, *332*, 473–504.
- Campbell, C. S. (2006), Granular material flows - an overview, *Powder Technology*, *162*, 208–229, doi:10.1016/j.powtec.2005.12.008.
- Carneiro, M. V., T. Pähtz, and H. J. Herrmann (2011), Jump at the onset of saltation, *Physical Review Letters*, *107*(9), 098,001, doi:10.1103/PhysRevLett.107.098001.
- Carneiro, M. V., N. A. M. Araújo, T. Pähtz, and H. J. Herrmann (2013), Midair collisions enhance saltation, *Physical Review Letters*, *111*(5), 058,001, doi:10.1103/PhysRevLett.111.058001.
- Charru, F., B. Andreotti, and P. Claudin (2013), Sand ripples and dunes, *Annual Review of Fluid Mechanics*, *45*, 469–493, doi:10.1146/annurev-fluid-011212-140806.
- Cheng, N. S. (1997), Simplified settling velocity formula for sediment particle, *Journal of Hydraulic Engineering*, *123*(2), 149–152, doi:doi:10.1061/(ASCE)0733-9429(1997)123:2(149).
- Claudin, P., and B. Andreotti (2006), A scaling law for aeolian dunes on mars, venus, earth, and for subaqueous ripples, *Earth and Planetary Science Letters*, *252*, 30–44, doi:10.1016/j.epsl.2006.09.004.
- Creyssels, M., P. Dupont, A. O. el Moctar, A. Valance, I. Cantat, J. T. Jenkins, J. M. Pasini, and K. R. Rasmussen (2009), Saltating particles in a turbulent boundary layer: experiment and theory, *Journal of Fluid Mechanics*, *625*, 47–74, doi:10.1017/S0022112008005491.
- Durán, O., P. Claudin, and B. Andreotti (2011), On aeolian transport: Grain-scale interactions, dynamical mechanisms and scaling laws, *Aeolian Research*, *3*, 243–270, doi:10.1016/j.aeolia.2011.07.006.
- Durán, O., B. Andreotti, and P. Claudin (2012), Numerical simulation of turbulent sediment transport, from bed load to saltation, *Physics of Fluids*, *24*, 103,306, doi:10.1063/1.4757662.
- Durán, O., P. Claudin, and B. Andreotti (2014a), Direct numerical simulations of aeolian sand ripples, *Proceedings of the National Academy of Science*, *111*(44), 15,665–15,668, doi:10.1073/pnas.1413058111.
- Durán, O., B. Andreotti, and P. Claudin (2014b), Turbulent and viscous sediment transport: a numerical study, *Advances in Geosciences*, *37*, 73–80, doi:10.5194/adgeo-37-73-2014.
- Fourrière, A., P. Claudin, and B. Andreotti (2010), Bedforms in a turbulent stream: formation of ripples by primary linear instability and of dunes by nonlinear pattern coarsening, *Journal of Fluid Mechanics*, *649*, 287–328.
- Griebel, M., S. Knapek, and G. Zumbusch (2007), *Numerical Simulation in Molecular Dynamics: Numerics, Algorithms, Parallelization, Applications*, Springer.
- Hersen, P., S. Douady, and B. Andreotti (2002), Relevant length scale of barchan dunes, *Physical Review Letters*, *89*(26), 264,301.
- Hunt, J. C. R., S. Leibovich, and K. J. Richards (1988), Turbulent shear flows over low hills, *Quarterly Journal of the Royal Meteorological Society*, *114*, 1435–1470.
- Jackson, P. S., and J. C. R. Hunt (1975), Turbulent wind flow over a low hill, *Quarterly Journal of the Royal Meteorological Society*, *101*, 929–955.
- Julien, P. Y. (1995), *Erosion and Sedimentation*, Press Syndicate of the University of Cambridge.
- Kawamura, R. (1951), Study of sand movement by wind, in *Translated (1965) as University of California Hydraulics Engineering Laboratory Report HEL 28 Berkeley*.
- Kind, R. J. (1976), A critical examination of the requirements for model simulation of wind-induced erosion/deposition phenomena such as snow drifting, *Atmospheric Environment*, *10*(3), 219–227, doi:10.1016/0004-6981(76)90094-9.
- Kok, J. F., and N. O. Renno (2009), A comprehensive numerical model of steady state saltation (comsalt), *Journal of Geophysical Research*, *114*, D17,204, doi:10.1029/2009JD011702.
- Kok, J. F., E. J. R. Parteli, T. I. Michaels, and D. B. Karam (2012), The physics of wind-blown sand and dust, *Reports on Progress in Physics*, *75*, 106,901.
- Kroy, K., G. Saueremann, and H. J. Herrmann (2002a), Minimal model for aeolian sand dunes, *Physical Review E*, *66*, 031,302, doi:10.1103/PhysRevE.66.031302.
- Kroy, K., G. Saueremann, and H. J. Herrmann (2002b), A minimal model for sand dunes, *Physical Review Letters*, *64*, 054,301, doi:10.1103/PhysRevLett.88.054301.
- Lämmel, M., D. Rings, and K. Kroy (2012), A two-species continuum model for aeolian sand transport, *New Journal of Physics*, *14*, 093,037, doi:10.1088/1367-2630/14/9/093037.
- Lettau, K., and H. H. Lettau (1978), Exploring the world’s driest climate, in *IES Report*, vol. 101, pp. 110–147.
- Ma, G. S., and X. J. Zheng (2011), *The European Physical Journal E*, *34*(5), 1–11, doi:10.1140/epje/i2011-11054-3.
- Narteau, C., D. Zhang, O. Rozier, and P. Claudin (2009), Setting the length and time scales of a cellular automaton dune model from the analysis of superimposed bed forms, *Journal of Geophysical Research*, *114*(F3), F03,006, doi:10.1029/2008JF001127.
- Owen, P. R. (1964), Saltation of uniform grains in air, *Journal of Fluid Mechanics*, *20*(2), 225–242.

- Pähtz, T., J. F. Kok, and H. J. Herrmann (2012), The apparent roughness of a sand surface blown by wind from an analytical model of saltation, *New Journal of Physics*, *14*(4), 043,035, doi:10.1088/1367-2630/14/4/043035.
- Pähtz, T., J. F. Kok, E. J. R. Parteli, and H. J. Herrmann (2013), Flux saturation length of sediment transport, *Physical Review Letters*, *111*(21), 218,002, doi:10.1103/PhysRevLett.111.218002.
- Pähtz, T., E. J. R. Parteli, J. F. Kok, and H. J. Herrmann (2014), Analytical model for flux saturation in sediment transport, *Physical Review E*, *89*(5), 052,213, doi:10.1103/PhysRevE.89.052213.
- Pähtz, T., O. Durán, T.-D. Ho, A. Valance, and J. F. Kok (2015), The fluctuation energy balance in non-suspended fluid-mediated particle transport, *Physics of Fluids*, *27*(1), 013,303, doi:10.1063/1.4905911.
- Parteli, E. J. R., and H. J. Herrmann (2007a), Saltation transport on mars, *Physical Review Letters*, *98*, 198,001, doi:10.1103/PhysRevLett.98.198001.
- Parteli, E. J. R., and H. J. Herrmann (2007b), Dune formation on the present mars, *Physical Review E*, *76*, 041,307, doi:10.1103/PhysRevE.76.041307.
- Parteli, E. J. R., O. Durán, and H. J. Herrmann (2007), Minimal size of a barchan dune, *Physical Review E*, *75*, 011,301, doi:10.1103/PhysRevE.75.011301.
- Parteli, E. J. R., O. Durán, H. Tsoar, V. Schwämmle, and H. J. Herrmann (2009), Dune formation under bimodal winds, *Proceedings of the National Academy of Science*, *106*(52), 22,085–22,089, doi:10.1073/pnas.0808646106.
- Parteli, E. J. R., J. S. Andrade, and H. J. Herrmann (2011), Transverse instability of dunes, *Physical Review Letters*, *107*, 188,001, doi:10.1103/PhysRevLett.107.188001.
- Parteli, E. J. R., K. Kroy, H. Tsoar, J. S. Andrade, and T. Pöschel (2014), Morphodynamic modeling of aeolian dunes: Review and future plans, *The European Physical Journal Special Topics*, *223*(11), 2269–2283, doi:10.1140/epjst/e2014-02263-2.
- Pelletier, J. D. (2009), Controls on the height and spacing of eolian ripples and transverse dunes: A numerical modeling investigation, *Geomorphology*, *105*(3-4), 322–333, doi:10.1016/j.geomorph.2008.10.010.
- Rasmussen, K. R., and M. Sørensen (2008), Vertical variation of particle speed and flux density in aeolian saltation: Measurement and modeling, *Journal of Geophysical Research*, *113*, F02S12, doi:10.1029/2007JF000774.
- Rioual, F., A. Valance, and D. Bideau (2000), Experimental study of the collision process of a grain on a two-dimensional granular bed, *Physical Review E*, *62*, 2450, doi:10.1103/PhysRevE.62.2450.
- Rioual, F., A. Valance, and D. Bideau (2003), Collision process of a bead on a two-dimensional bead packing: Importance of the inter-granular contacts, *Europhysics Letters*, *61*(2), 194, doi:10.1209/epl/i2003-00212-8.
- Sauermann, G., K. Kroy, and H. J. Herrmann (2001), A continuum saltation model for sand dunes, *Physical Review E*, *64*, 31,305, doi:10.1103/PhysRevE.64.031305.
- Schmeeckle, M. W. (2014), Numerical simulation of turbulence and sediment transport of medium sand, *Journal of Geophysical Research: Earth Surface*, *119*(6), 1240–1262, doi:10.1002/2013JF002911.
- Schwämmle, V., and H. J. Herrmann (2003), Geomorphology: Solitary wave behaviour of sand dunes, *Nature*, *426*, 619–620, doi:10.1038/426619a.
- Shao, Y. (2008), *Physics and modelling of wind erosion*, Kluwer Academy, Dordrecht, Amsterdam.
- Sørensen, M. (1991), An analytic model of wind-blown sand transport, *Acta Mechanica Supplement*, *1*, 67–81.
- Sørensen, M. (2003), On the rate of aeolian sand transport, *Geomorphology*, *59*, 53–62.
- Spies, P. J., I. K. McEwan, and G. R. Butterfield (2000), One-dimensional transitional behaviour in saltation, *Earth Surface Processes and Landforms*, *25*(5), 505–518.
- Ungar, J. E., and P. K. Haff (1987), Steady state saltation in air, *Sedimentology*, *34*, 289–299.

Corresponding author: Thomas Pähtz, Institute of Physical Oceanography, Ocean College, Zhejiang University, 310058 Hangzhou, China. (0012136@zju.edu.cn)